Electronic Materials Letters, Vol. 1, No. 1 (2005), pp. 19-25

Metamorphic HEMT Devices and MMICs' for Millimeter-wave System Applications

Kyung Ho Lee*, Dong Min Kang, Ju Yeon Hong, Jae Yeob Shim, and Hyung-Sup Yoon

InP IC Team Basic Research Laboratory, Electronics and Telecommunications Research Institute (ETRI)
Daejeon 305-350, Korea

We present the device and integrated circuit (IC) characteristics of GaAs metamorphic high electron mobility transistors (MHEMT). A 0.15×100 mm^2 MHEMT device shows a drain saturation current of 480 mA/mm, an extrinsic transconductance of 830 mS/mm, and a threshold voltage of -0.65 V. The obtained cut-off frequency and maximum frequency of oscillation are 141 and 243 GHz, respectively. The noise performance is excellent; minimum noise figures of 0.79 and 0.64 dB, and associated gains of 10.56 and 12.4 dB at 26 GHz for 0.15 mm-long T-gate and 0.1 mm-long G-gate power MHEMTs, respectively, with In content of 53 % in InGaAs channel. Using the MHEMT technology with a 0.15 mm-long T-gate, we designed and fabricated monolithic microwave integrated circuits (MMICs) on 4-inch MHEMT wafers. The MMIC performance for a power amplifier and a down mixer for 76-77 GHz band is presented. These devices and ICs can be used for wireless telecommunications systems and also in millimeter-wave sensor systems for commercial or military applications.

Keywords: GaAs, InP, millimeter-wave, MHEMT, T-gate, G-gate, MMIC

1. INTRODUCTION

There is strong interest in anticipating the ideal 4G telecommunications system as well as its frequency and speed so as to comply with the ever-growing demand for mobile and high volume communications systems and services. As subscriber demand becomes more rigorous, there are more challenges for the system technology and the corresponding components technology with regard to speed and volume of communications. At millimeter-wave frequencies, as large spectrums of bandwidth are available, the allocation of commercial frequency bands at these frequencies has attracted interest for the development of commercial communications systems to meet such challenges. Also, as antenna size is proportional to wavelength, the antenna size can be reduced significantly at millimeter-wave frequencies compared to microwave frequencies for the same resolution. Or the resolution becomes better at millimeter-wave frequencies than at microwave frequencies for the same antenna size.

For the realization of millimeter-wave communications systems, the concurrent development of low-cost circuits and modules as components for those systems is necessary. In this context, we present some of the millimeter-wave monolithic microwave integrated circuit (MMIC) and module prototypes developed for the next generation wireless telecommunications systems. MMICs' have been designed and fabricated using ETRI's own high electron mobility transistor (HEMT) technology, utilizing 4-inch metamorphic HEMT (MHEMT) wafers. Although InP HEMT having an InAlAs/InGaAs heterostructure grown on an InP substrate provides higher electron mobility, higher gain, lower noise, and higher frequency performances than GaAs-based HEMT[1,2], the InP wafer has several drawbacks including size limitation, fragility, and high price. This has recently led to the active development of MHEMT having an InAlAs/

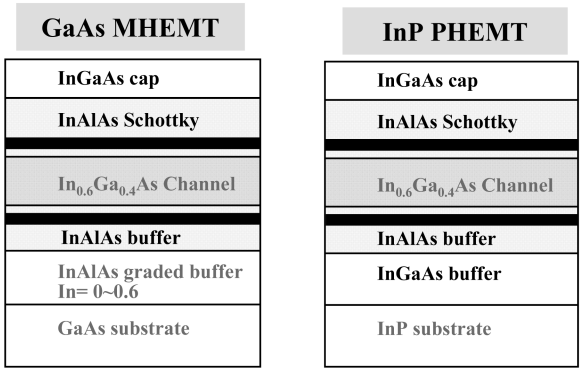

(a) GaAs MHEMT (b) InP PHEMT

Fig. 1. Schematic comparison of structures of (a) GaAs MHEMT and (b) InP PHEMT.

*Corresponding author: kh1259@etri.re.kr

InGaAs heterostructure grown on a GaAs substrate by use of an InAlAs buffer, as schematically shown in Fig. 1.

Schottky and channel layers are identical for both structures. Graded InAlAs buffer is used to gradually compensate the lattice mismatch between substrate and channel in MHEMT. Recently, MHEMT devices show electrical performances that are compatible with those of InP PHEMT[3,4]. Thus, MHEMT is becoming a crucial device in MMICs' for high power and low noise applications[5-7].

As MMICs' have been primarily developed for use in wireless telecommunications systems, they can also be used in the millimeter-wave sensor systems, such as surveillance robots, automotive collision avoidance systems(ACAS), and image sensing for commercial and military use. Among these applications, the millimeter-wave automotive collision avoidance radar system is a key technology for future adaptive cruise control(ACC) systems. With increased awareness and interest in safety issues pertaining to vehicular transportation, a variety of obstacle detectors has been researched and developed. In particular, a forward looking automotive radar has received special attention as it is considered to be an essential element of a vehicular safety system[8,9].

A promising way to meet the stringent cost requirements of these systems is the use of MMICs' based on MHEMT technology for good circuit performance with a further reduction of chip size.

In this context, we developed InGaAs/InAlAs/GaAs MHEMT devices having a 0.15 μm-long T-gate and 0.1 μm-long Γ-gate. Using the 0.15 μm-long T-gate MHEMT, we developed some key MMICs' for applications demanding low cost and high performance millimeter-wave systems.

2. MHEMT DEVICE CHARACTERISTICS

The MHEMT structures were grown by molecular beam epitaxy (MBE). The epitaxial structures of the 0.15 μm-long T-gate MHEMT are schematically shown in Fig. 2.

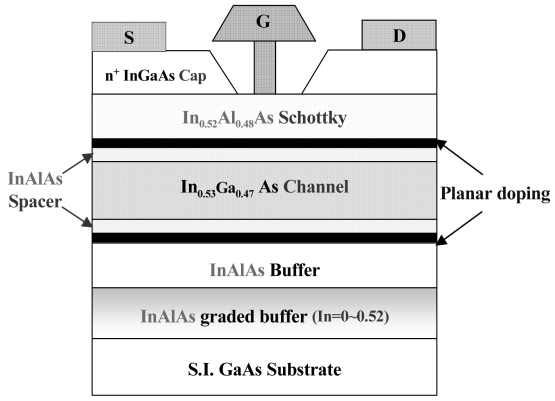

Fig. 2. Schematic representation of the epitaxial structure of T-gate MHEMT.

For the T-gate shown in Fig. 2, the length of the gate foot on the Schottky layer is 0.15 μm. The gate has a Γ-shape and the foot length is 0.1 μm for the 0.1 μm Γ-gate MHEMT described above. For both types, the width of the gate head is greater than 1 μm. This wide head shape lowers the gate resistance and enhances electrical properties, especially noise performance[10].

Scanning electron microscope images of 0.15 μm T-gate and 0.1 μm Γ-gate MHEMT are shown in Fig. 3. The gate structures were patterned by electron beam direct writing lithography using a Leica EBPG 5000+ system and Ti/Pt/Au gate metals were deposited by an electron beam evaporation technique and then lifted-off. The fabrication process has been described in detail elsewhere[10,11,12].

2.1. Electrical performance of 0.15 μm T-gate MHEMT

The Schottky current-voltage (I-V) characteristics of the 0.15 μm T-gate MHEMT devices were measured at room temperature. The ideality factor (n) of the Schottky diode calculated from the measured forward I-V characteristic was 1.42 and the devices showed good Schottky diode character-

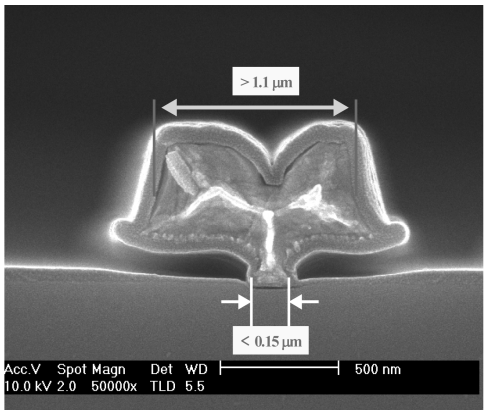

(a) SEM image of 0.15 μm-long T-gate MHEMT. Note the width of the gate head is greater than 1.1 μm.

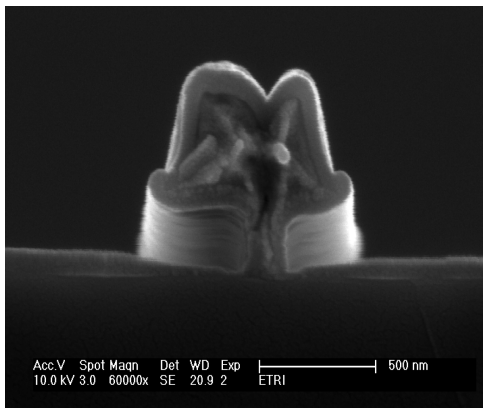

(b) SEM image of 0.1μm-long Γ-gate MHEMT[10]

Fig. 3. SEM images of (a) 0.15 μm T-gate and (b) 0.1 μm Γ-gate MHEMT.

istics. A considerably high breakdown voltage of -8.3V, at which the gate current reaches 1mA/mm, was also obtained for the T-gate MHEMT devices with a high In content of 0.53 in the lattice-matched $In_{0.53}Ga_{0.47}As$ channel layer.

Figure 4 shows drain currents as a function of source-to-drain voltage for the 0.15×100 μm^2 T-gate MHEMT devices. The MHEMT devices exhibit complete pinch-off characteristics. The measured drain saturation current is 48 mA at a source-to-drain voltage of 2 V and a source-to-gate voltage of 0 V.

Figure 5 shows the extrinsic transconductance and the drain current (I_{ds}) as a function of gate-to-source voltage (V_{gs}) at a source-to-drain voltage of 1.5 V for the 0.15×100 μm^2 T-gate MHEMT device. The measured threshold voltage is -0.65 V. The measured maximum extrinsic transconductance is 830 mS/mm at a gate-to-source voltage of -0.13 V.

The *s*-parameters were measured on a 4-inch wafer using a Cascade microwave probe station and an HP 8510C network analyzer ranging from 1 to 50 GHz. Figure 6 shows the measured current gain ($|h_{21}|$) and MSG/MAG as a function of frequency of a 0.15×100 μm^2 T-gate MHEMT device. The cut-off frequency (f_T) was calculated by the extrapolation of $|h_{21}|$ to unity with a -20 dB/decade slope, and the maximum frequency of oscillation (f_{max}) was obtained by parallel shifting of -20 dB/decade slope to the MSG/MAG plot. The obtained f_T and f_{max} for the T-gate MHEMT device were 141 and 243 GHz, respectively.

The noise characteristics of the T-gate MHEMT devices were examined. The noise figure measurements have been carried out in a frequency range between 26 GHz and 40 GHz using an HP 8510C network analyzer, an HP 8970B noise figure meter, and an ATN NP5 noise parameter test set. Figure 7 shows the minimum noise figure (F_{min}) and the associated gain (G_{as}) as a function of frequency at I_{ds}= 7.4 mA and V_{ds} = 1V of the 0.15×100 μm^2 T-gate MHEMT device. F_{min} of 0.79 dB and G_{as} of 10.56 dB are measured at 26 GHz. At 40 GHz, the measured NF_{min} and G_{as} are 1.21 dB and 6.41 dB, respectively. Considering the power MHEMT structure with an In content of 53% in the InGaAs channel, these noise characteristics are excellent. As shown in Fig. 3

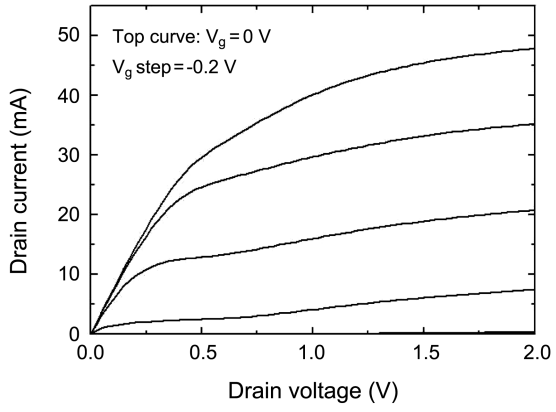

Fig. 4. Current-voltage characteristic for a 0.15 μm T-gate MHEMT. The gate-source voltage was changed from 0 to -1.2 V with a -0.2 V step.

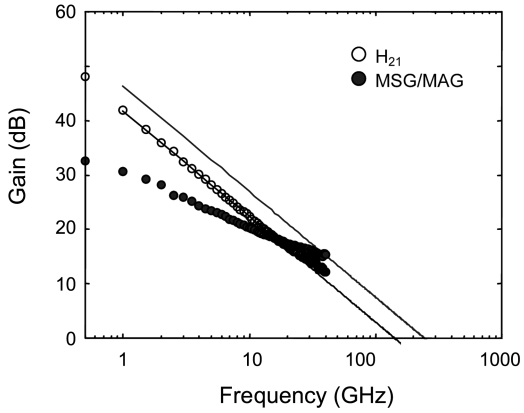

Fig. 6. Frequency dependence of the current gain ($|h_{21}|$) for a 0.15 μm MHEMT under a source-to-drain voltage (V_{ds}) of 1.5 V and a gate-to-source voltage (V_{gs}) of -0.35 V.

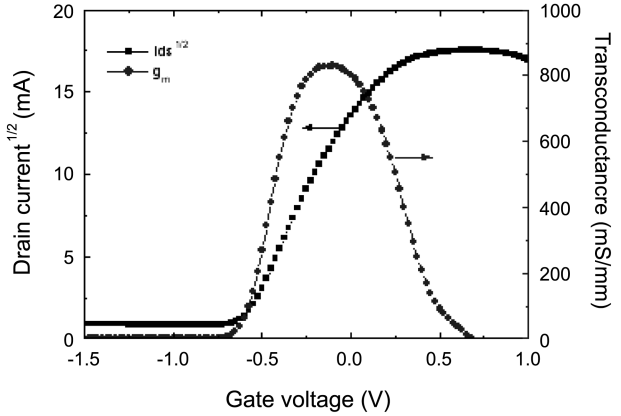

Fig. 5. Drain current and transconductance as a function of gate voltage of a 0.15 μm T-gate MHEMT biased at a drain voltage of 1.5 V.

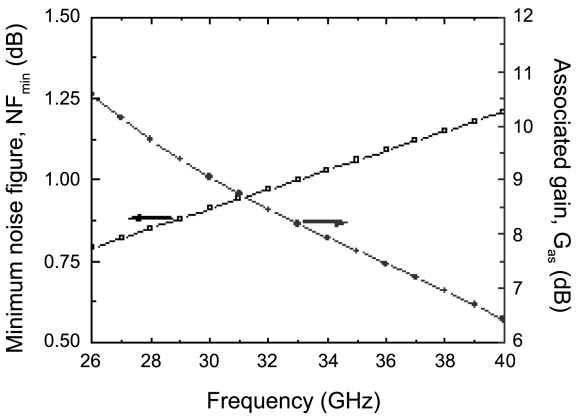

Fig. 7. Minimum noise figure, NF_{min}, and associated gain, G_{as}, as a function of frequency at V_{ds}=1V and I_{ds}= 7.4 mA of a 0.15×100 μm^2 T-gate MHEMT

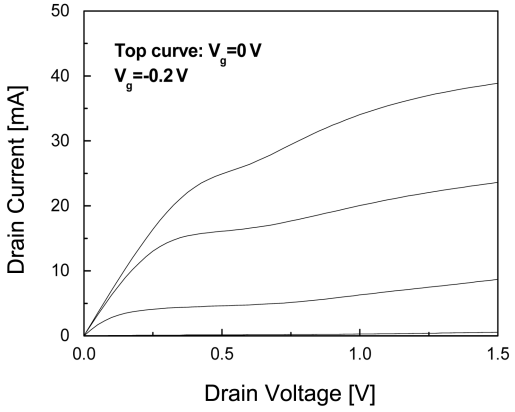

Fig. 8. I-V characteristics for 0.1×100 μm^2 Γ-gate MHEMT.

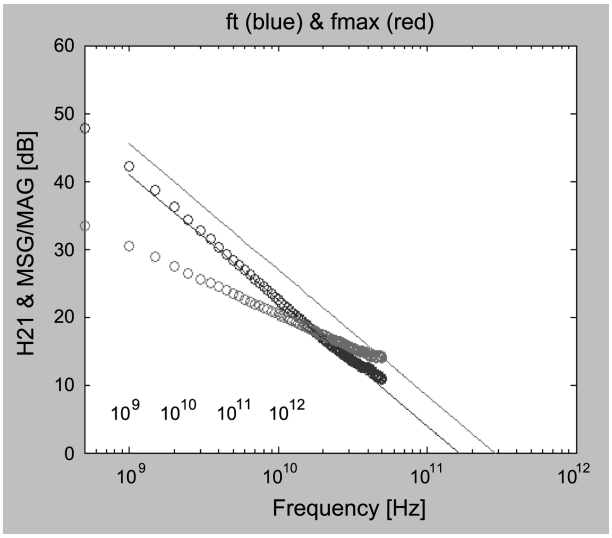

Fig. 9. Typical frequency dependence of the current gain ($|h_{21}|$) for 0.1×100 μm^2 Γ-gate MHEMT.

(a), the wide head T-shaped gate with an aspect ratio of head-to-gate provides a significant reduction of gate resistance. Thus, this low noise performance can be attributed to the drastic reduction of gate resistance by the T-shaped gate with a wide head[13] and improved device performance[14].

2.2. Electrical performance of 0.1 μm Γ-gate MHEMT

Hall measurements of the 0.1 μm-long Γ-gate MHEMT structure yielded an electron sheet density of n_s=3.5×10^{12}cm^{-2} and mobility of μ_H=9,100cm^2/V · s at 300 K. Figure 8 shows the drain current as a function of source-to-drain voltage (V_{ds}) for 0.1×100 μm^2 Γ-gate MHEMT devices fabricated by wet recess etching with a solution of succinic acid : H_2O_2. MHEMT devices exhibit a good pinch-off characteristic at a drain voltage of 1.5 V. The drain saturation current, I_{dss}, measured at V_{ds}=1.5 V and V_{gs}=0 V is 38 mA.

The *s*-parameters for the 0.1×100μm^2 Γ-gate MHEMT devices were measured on a wafer from 1 to 50 GHz by

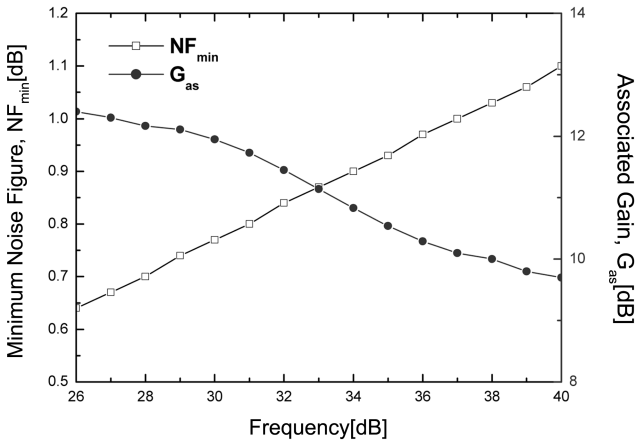

Fig. 10. Minimum noise figure, NF_{min}, and associated gain, G_{as}, as a function of frequency at V_{ds}=1V and I_{ds}=7 mA for 0.1×100 μm^2 MHEMT with wide head Γ-gate

using a Cascade microwave probe station and an HP 8510C network analyzer.

The measured current gain, h_{21}, and MSG/MAG as a function of frequency for the MHEMT device are shown in Fig. 9. f_T and f_{max} were measured as described in 2.1. and were 165 and 275 GHz, respectively, as shown in Fig. 9.

NF_{min} was measured as described in 2.1. NF_{min} at 26 GHz exhibits a minimum at drain current of 7 mA for V_{ds}=1V. Figure 10 shows NF_{min} and G_{as} as a function of frequency measured at I_{ds}=7 mA and V_{ds}=1V for 0.1×100 μm^2 Γ-gate MHEMT. NF_{min} measured at 26 GHz is 0.64 dB with G_{as} of 12.4 dB. NF_{min} measured at 40 GHz is 1.1 dB with associated gain of 9.7 dB. This noise data constitute the lowest values ever reported for power MHEMT devices with an InGaAs channel of 53 % In[10]. This excellent noise performance is attributed to the low gate resistance arising from the wide head Γ-gate and the improved RF performance of the MHEMT device.

2.3. MMICs' electrical performance with 0.15 μm T-gate MHEMT

As introduced in Section I), the potential of MHEMTs for high performance, high power, and low noise applications has recently been demonstrated. It has also been shown that the electrical transport properties of the MHEMT structure are largely affected by the mole fraction of the InGaAs channel layer and the metamorphic buffer layer. Notably, reproducible devices should be obtained for the application of MHEMT to MMICs' with the use of a reliable fine line gate lithography process to satisfy these requirements. In this paper, MMICs' with passivated 0.15 μm T-gate MHEMTs were fabricated by combining a wide head T-shaped gate. This was accomplished using a dose split method of electron beam lithography and a highly selective recess etch process based on succinic acid. These MMICs' are developed for

application as an RF front-end in automotive collision avoidance systems (ACAS).

Figure 11 shows a generalized block diagram of the RF front-end of ACAS.

In this paper, we introduce a power amplifier (PA) MMIC in the transmitter and a down-mixer (DM) MMIC in the receiver for a RF front-end of an ACAS.

2.3.1. Power amplifier (PA) MMIC

A 4-stage PA was designed using MHEMT devices of 2-finger 100μm (2f100) and 4-finger 200μm (4f200). Figure 12 shows the circuit schematic and a photograph of the fabricated PA MMIC.

In order to increase the stability of the MHEMT device, negative fee dBack was employed by a resistor network. The first two stages used MHEMTs with a 100 μm gate width and operated as class A amplifiers for gain consideration, while the last two stages employed 200 μm devices for power and efficiency requirements and operated at class A. The detailed design methodology has been presented elsewhere[11].

On-wafer measurement was performed using an HP PNA N5250A 110 GHz network analyzer. The PA demonstrated a measured small signal gain of over 20 dB from 76 to 77 GHz with 15.5 dBm output power. The chip size was 2×2 mm^2. Figure 13 presents the on-wafer measurement results of the fabricated PA MMIC.

Our PA results demonstrated the highest output power and gain among all the reported 77 GHz MMIC PAs for automotive radar systems using 0.15 μm GaAs HEMTs[11, 15-19].

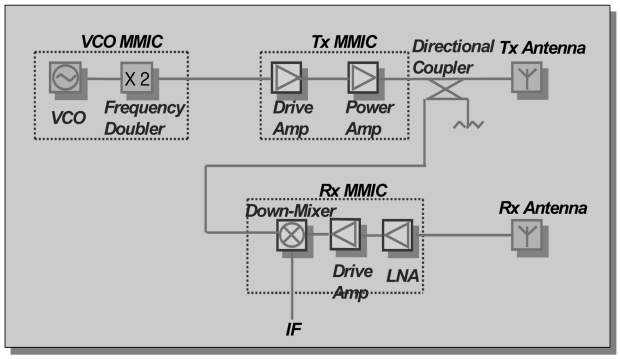

Fig. 11. Block diagram of RF front-end of ACAS.

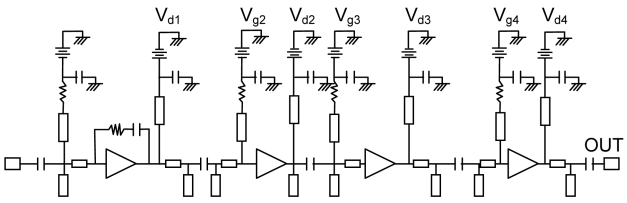

(a) Circuit schematic of fabricated PA MMIC using 0.15 μm T-gate MHEMT

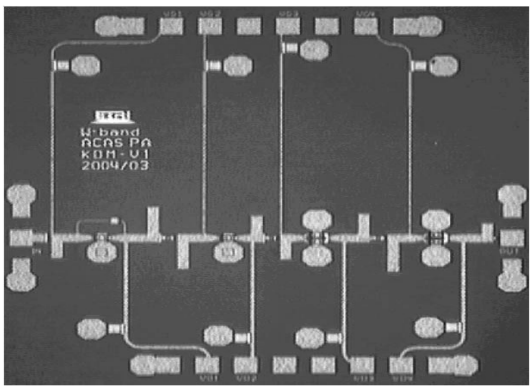

(b) Photograph of fabricated PA MMIC using 0.15μm T-gate MHEMT

Fig. 12. Schematic circuit diagram and photograph of fabricated 4-stage PA MMIC using 0.15μm T-gate MHEMT.

2.3.2. Down Mixer(DM) MMIC

The W-band harmonic drain mixer is designed to down-convert 75.1~82 GHz RF by mixing with the second har-

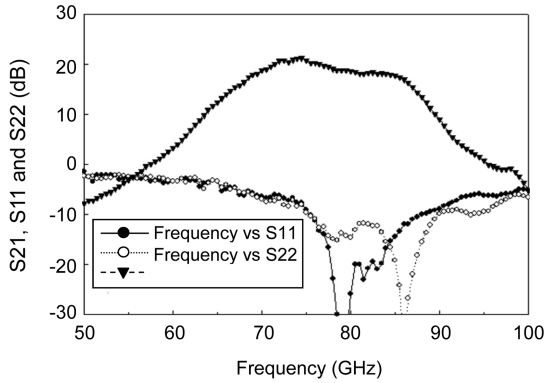

(a) Small signal gain (S21), input return loss (S11), and output return loss (S22) as a function of frequency (50 to 100 GHz) for the fabricated MMIC PA

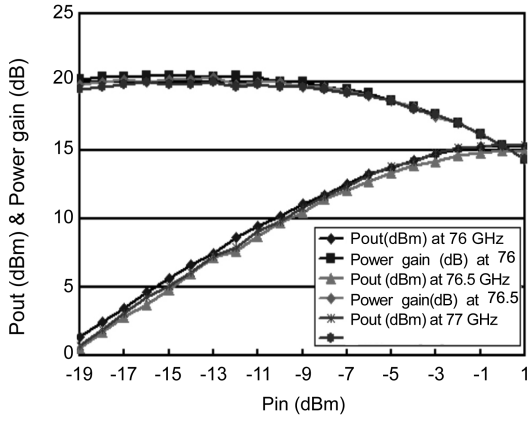

(b) Output power and power gain as a function of input power at 76 to 77 GHz 1 tone for the fabricated MMIC PA

Fig. 13. Measurement results of fabricated PA MMIC.

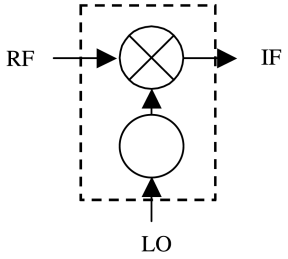

Fig. 14. Circuit diagram of MMIC harmonic mixer.

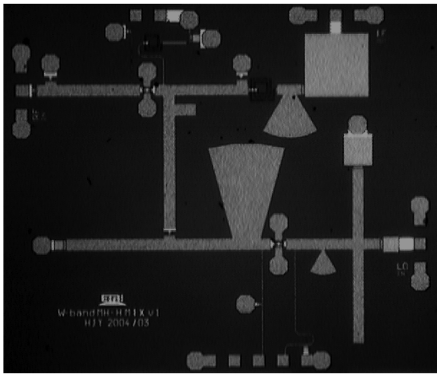

Fig. 15. Photograph of the fabricated harmonic mixer MMIC.

monic of a 37.5 GHz LO signal. For a common-source FET mixer, there are two different configurations, a gate mixer and a drain mixer. The drain mixer has a RF signal applied to the gate terminal and an LO signal applied to the drain terminal, while the gate mixer is operated with RF and LO signals applied at the gate terminal. Since the drain mixer is operated as a resistive mixer, the drain mixer has advantages of good LO-IF isolation characteristics and good RF suppression characteristics. Figure 14 shows the designed circuit diagram of the harmonic mixer.

The harmonic mixer MMIC is composed of a drain mixer and a frequency doubler. The output of the frequency doubler is connected with the drain terminal of the drain mixer. As FET of the drain mixer is biased at zero bias, dc power consumption of the harmonic mixer is very low.

Figure 15 shows a photograph of the fabricated harmonic mixer MMIC. The chip size of the harmonic mixer MMIC is 2.6×2.3 mm^2. The harmonic mixer employs microstrip lines, thin film resistors, metal-insulated-metal capacitors, spiral inductors, and radial stubs as transmission structures, filter structures, and matching networks.

On-wafer conversion loss measurement of DM is performed with -13 dBm RF input power over 75.1~84 GHz. An Agilent model 83650B synthesizer is used to provide an LO signal at 37.5 GHz, while the IF output is measured with an Agilent 8565EC spectrum analyzer.

The measured results shown in Fig. 16 indicate that the conversion loss is 10.4~12 dB over 75.1~82 GHz RF frequency with 5 dBm LO power. The biases are at Vds_1=0V, Vgs_1 = -0.7 V, Vds_2 = 1.5 V, Vgs_2 = -0.7 V. (Vds_1, Vgs_1 are biases of the mixer and Vds_2, Vgs_2 are biases of the doubler, respectively.)

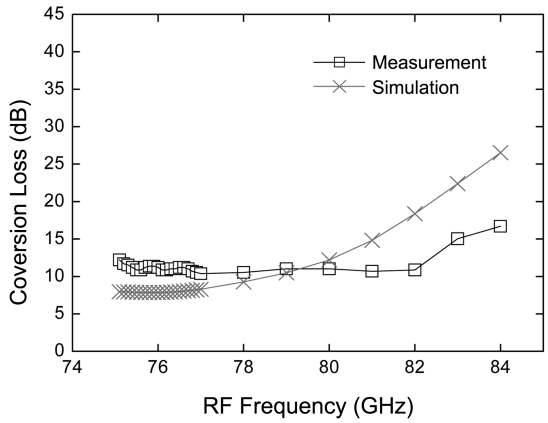

Fig. 16. Simulated and measured results of conversion loss above 75~84 GHz with 5 dBm LO power level

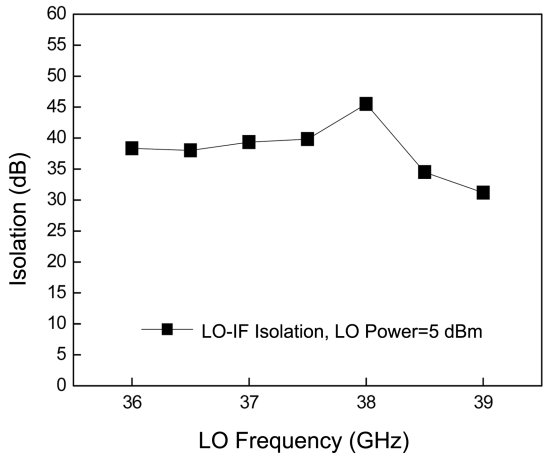

Fig. 17. Measured results of LO-IF Isolation above 36~39 GHz with 5 dBm LO power level.

The measured result of LO to IF isolation is about 35 dB, and the measured result of RF fundamental suppression is around 65 dBc. The measured results of the LO-IF isolation of the harmonic mixer are shown in Fig. 17.

The conversion loss and isolation characteristics are among the best demonstrated from a 4-inch InAlAs/InGaAs MHEMT harmonic mixer MMICs operating at W-band frequency.

3. CONCLUSION

The DC, RF, and noise performances of a 0.15 μm gate-length T-gate and a 0.1 μm gate-length Γ-gate wide head MHEMTs with a double-doped InAlAs/InGaAs structure were investigated. The 0.15×100 μm^2 T-gate MHEMT

devices showed an extrinsic transconductance of 830mS/mm, and a threshold voltage of -0.64 V. The cut-off frequency and the maximum frequency of oscillation were measured as 141 and 243 GHz, respectively. A very low minimum noise figure of 0.79 dB and an associated gain of 10.56 dB were obtained at 26 GHz. These 0.15 μm power MHEMT devices can be applicable for the fabrication of transceivers for millimeterwave system applications. The MHEMTs showed NF_{min} of 0.64 dB and an associated gain of 12.4 dB at 26 GHz. This noise data is the lowest value ever reported for power MHEMT devices. The low noise performance can be explained by the drastic reduction of the gate resistance by the T-shaped gate with a wide head and improved device performance. This device is applicable for medium power and low-noise MMIC fabrication. These MHEMT devices were successfully used for the development of an MMIC chip set for automotive radar systems using ETRI's 0.15 μm InGaAs/InAlAs/GaAs MHEMT technology on a 4-inch 100 μm thick GaAs substrate. The PA demonstrated a measured small signal gain of over 20 dB from 76 to 77 GHz with 15.5 dBm output power. The chip size was 2×2 mm^2. The conversion loss of the down-mixer was 10.4~12 dB over 75.1~82 GHz RF frequency with 5 dBm LO power. The measured result of LO to IF isolation is about 35 dB and the measured results of RF fundamental suppression is around 65 dBc. The chip size of the harmonic mixer MMIC is 2.6×2.3 mm^2. These MMICs are suitable for 77 GHz automotive radar systems and related applications in the W-band.

REFERENCES

1. M. Y. Kao, K. H. G. Duh, P. Ho, and P. C. Chao, *IEDM Tech. Dig*. p. 907 (1994).
2. P. M. Smith, S. -M. J. Liu, M. -Y. Kao, P. Ho, S. C. Wang, K. H. G. Duh, S. T. Fu, and P. C. Chao, *IEEE Microwave Guided Wave Lett.* **5**, 230-232 (1995).
3. H. S. Yoon *et al*., *International Conference on Indium Phosphide and Related Materials Proceeding*, pp. 114-117 (2003).
4. K. Shinohara *et al*., *Jpn. J. Appl. Phys.* **41**, L437-L439 (2002).
5. M. Zaknoune, B. Bonte, C. Gaquiere, Y. Cordier, Y. Druelle, and Y. Crosnier, *IEEE Electron Device Lett*. **19**, 345-347 (1998).
6. C. S. Whelan, W. E. Hoke, R. A. MacTaggart, S. M. Lardizabal, P. S. Lyman, P. F. Marsh, and T. E. Kazior, *Electron Device Lett*. **21**, 5-8 (2000).
7. J. Y. Shim, H-S. Yoon, S. J. Kim, J. Y. Hong, W. J. Chang, D. M. Kang, J-H. Lee, and K. H. Lee, *J. Korea Phys. Soc*. **41**, 528-532 (2002).
8. K. Kamozaki *et al*., *GaAs IC Symp. Digest,* pp. 275-278 (1997).
9. J. Udomoto *et al*., *IEEE MTT-S Digest,* pp. 2229-2232 (2003).
10. H. S. Yoon, J. H. Lee, J. Y. Shim, J. Y. Hong, D. M. Kang, and K. H. Lee, *International Conference on Indium Phosphide and Related Materials Proceeding,* pp. 114-117 (2005).
11. D. M. Kang, J. Y. Hong, J. Y. Shim, J. -H. Lee, H. -S. Yoon, and K. H. Lee, *ETRI Journal* **27**, 133-139 (2005).
12. J. Y. Shim, H. S. Yoon, D. M. Kang, J. Y. Hong, and K. H. Lee, *to be published in ETRI Journal* (2005).
13. J. Y. Shim, H. -S. Yoon, S. J. Kim, J. Y. Hong, W. J. Chang, D. M. Kang, J. -H. Lee, and K. H. Lee, *J. Korea Phys. Soc*. **41**, 528-532 (2002).
14. H. Fukui, *IEEE Trans. Electron Devices* **26**, 1032-1037 (1979).
15. A. Tessmann *et al*., *GaAs IC Symp. Digest,* pp. 207-210 (1999).
16. H. Kondoh *et al*., *GaAs IC symp. Digest,* pp. 211-214 (1999).
17. H. J. Siweris *et al*., *RFIC symp. Digest,* pp. 191-194 (2000).
18. H. J. Siweris *et al*., *IEEE Trans. On MTT* **46**, 2560-2567 (1998).
19. H. Y. Chang *et al*., *IEEE Microwave and Wireless Comp. Lett.* **13**, 143-145 (2003).